Flux-Quanta Injection for Nonreciprocal Current Control in a Two-Dimensional Noncentrosymmetric Superconducting Structure

Serafim Teknowijoyo, Sara Chahid, and Armen Gulian*

Advanced Physics Laboratory, Institute for Quantum Studies, Chapman University, Burtonsville, Maryland 20866, USA

(Received 30 November 2022; revised 13 February 2023; accepted 12 July 2023; published 25 July 2023)

We designed and experimentally demonstrated a four-terminal superconducting device, a "quadristor," that can function as a nonlatching (reversible) superconducting switch from the diode regime to the resistive state by application of a control current much smaller than the main transport current. The device uses a vortex-based superconducting-diode mechanism that is switched back and forth via the injection of flux quanta through auxiliary current leads. Our finding opens a new research area in the field of superconducting electronics.

DOI: 10.1103/PhysRevApplied.20.014055

I. INTRODUCTION

Simultaneous breaking of time-reversal and inversion symmetries generates the superconducting-diode effect [1–8]. The time-reversal symmetry can be broken via an externally applied magnetic field or internal inclusions of magnetic microclusters [9], while inversion symmetry can be broken in several ways [4,6,10–23].

The recent spike of research in the area of superconducting diodes paves a road towards the future practical application of these novel devices in superconducting electronics. Moreover, it inspires substantiated hopes that the next stages of work, in analogy with semiconductor electronics, will be accomplished by the development of superconducting transistors [24]. By a "transistor" we refer to a regulated diode, whose resistive state can be controlled by an externally applied signal exerting much less power than the one it controls. In this report, we introduce such a device. Because of the specifics of superconductivity, where the devices are generally current biased, the controlling agent in our design is a current supplied by two closely located auxiliary leads. This justifies the term "quadristor": two leads for the transport current and two leads for controlling it. Via this relatively small control current, the diode properties of the quadristor can be turned *off* and *on* on demand without a noticeable latching effect and the device can function as a fast switch or as a signal controller or amplifier.

A. The idea of a quadristor

The main idea of the quadristor design stemmed from a hypothesis that the underlying mechanism of the diode effect in certain cases is based on vortex-lattice dynamics in the active area of the bridge. Indeed, during our previous stage of research [23], it was observed that the resistive state of the diode corresponds roughly to half of the normal-state value. In this case, the voltage-current dc measurements revealed a steplike pattern with a pronounced plateau, the height of which matches the ac voltage amplitude. In the literature, such voltage-current peculiarities are associated with vortex-pattern rearrangement (see, e.g., Ref. [25]). Thus, the quadristor idea capitalized on the suggestion that this rearrangement (and the associated resistance) can be triggered by the local insertion of vortices (flux quanta) externally. For the sake of vortex insertion, additional leads could be attached to the bridge's active area. To explore this quadristor concept experimentally, we fabricated the device described below.

II. EXPERIMENTAL

The device was fabricated by a multistage lithographic patterning of approximately-100-nm-thick Nb_3Sn films on sapphire substrates with $T_c > 17$ K, Fig. 1, with the geometry of the device shown in Fig. 2.

The comprehensive details of deposition and lithography are described elsewhere [23]. Ion milling affects the physical properties of bridges and reduces the critical temperature (see, e.g., Refs. [20,23]). The bridge reported here had $T_c \sim 4$ K. In this work, we did not attempt to restore T_c to 17 K via annealing as described in Ref. [23]. Rather, the bridge was used as prepared, because using the bridge with lower T_c allows one to deal with smaller critical currents, so that the transition to the normal state does not damage the bridge thermally.

*Corresponding author. gulian@chapman.edu

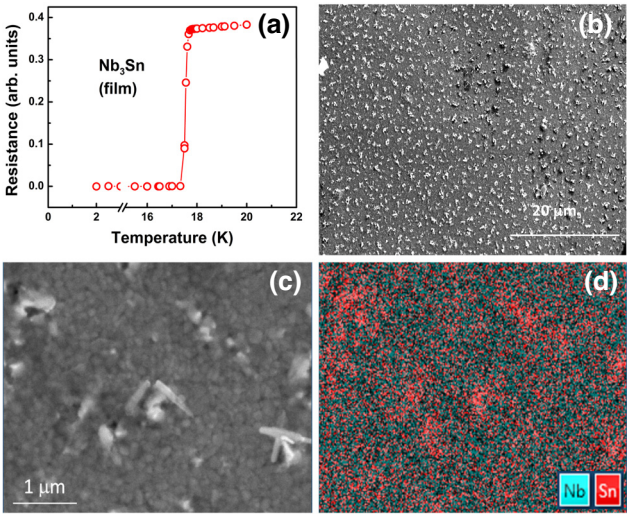

FIG. 1. Our Nb_3Sn film used for the device fabrication. (a) Resistive transition of the bridge. (b) SEM image showing randomly distributed agglomerations. (c) Higher-resolution SEM reveals the material's granularity, with an average grain size of about 200 nm, as well as larger features (closer to 1 μm). As the energy-dispersive-x-ray-spectroscopy microanalysis of the same area reveals in (d), these μm-size objects coincide with regions that show an excess amount of Sn.

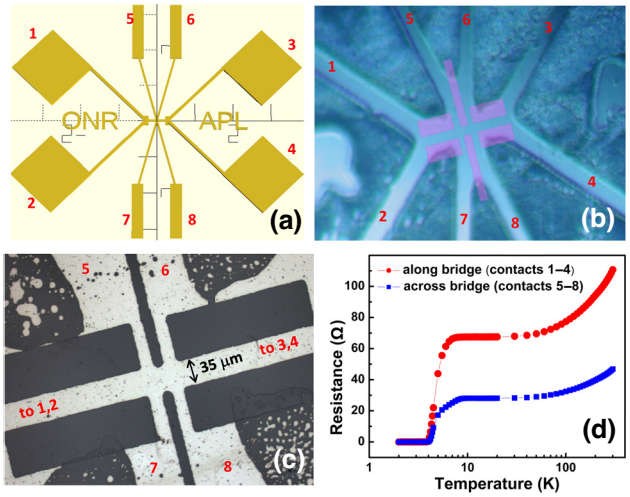

FIG. 2. Lithographically patterned quadristor. (a) The layout of the initial mask for the large-scale patterning via 3D-printer (Mars Elegoo-3), intertick distances correspond to 1 mm; the words "ONR"and "APL" were added to the authentic mask design for documentary purposes only, they represent the sponsor agency and the laboratory, respectively, and are visible partially on the real device pattern (next panel). (b) Central part of Nb_3Sn bridge formed by 3D-printed mask after the first ion milling. Afterwards it was covered by positive photoresist and a finer structure was defined by UV-light projection via the epifluorescence-microscope technique [23] (the illuminated area is shown by semitransparent rectangles) for subsequent final ion milling. (c) The central part (which serves as the active area) of the bridge after the final photolitographic processing. The light and dark areas correspond to the bridge and the sapphire substrate, respectively. Black dots inside the light area correspond to the agglomerations mentioned in the caption for Fig. 1(b). (d) The resistive transition of the bridge shown in (c). The top curve was measured via leads 1 and 3 (current) and leads 2 and 4 (voltage); the bottom curve was measured via leads 5 and 7 (current) and leads 6 and 8 (voltage).

III. RESULTS

A. Superconducting-diode effect

The fabricated bridge demonstrated voltage-current characteristics [Fig. 3(a)] similar to those reported in Ref. [23]. Measurements in a magnetic field revealed reasonably large values of $\Delta I = I^+ - I^-$ [Fig. 3(b)] and correspondingly a very robust diode effect (Fig. 4).

For this and all other measurements reported here, the direction of **H** is orthogonal to the surface of the film. Similarly to what was reported in Refs. [20,23], at positive values of the applied magnetic field, $I^+ < I^-$ and vice versa. The mechanism of a superconducting diode that reveals itself in our bridges was discussed in Ref. [23]. A small quantitative difference is that in the previous case the optimal magnetic field was about 100 Oe, and in this case the optimum is about 50 Oe: at 40 Oe, ΔI is decreased by 25%, while at 60 Oe, ΔI is decreased by 75%.

B. Quadristor

Our next observational step involved injecting the direct current via auxiliary leads 5 and 6. Our doing so generated localized current addition in the active area of the bridge, and, as shown in Fig. 5, switched the diode regime to a resistive state in both transport-current directions.

Very interestingly, there is no latching: the removal of this additional current through the auxiliary leads immediately restores the laminar flow (no vortices, no voltage) of the diode action, as Fig. 5 demonstrates. The effect occurred for both polarities of the external magnetic field.

IV. DISCUSSION

The mechanism of switching is based on nonequilibrium kinetics of vortices in the active area of the device, as explained in Fig. 6.

This explanation extends the modeling results reported previously for the case of the superconducting-diode effect in Nb_3Sn bridges [23]. In that case, during one of the half-periods of the alternating current, vortices enter through the edge with the lower Bean-Livingston barrier and their viscous motion generates a voltage and thus the finite resistance [Fig. 6(a)]. During the subsequent half-period, vortices are not able to rise through the higher Bean-Livingston barrier of the opposite edge, and no viscous motion occurs, keeping the voltage and resistance zero

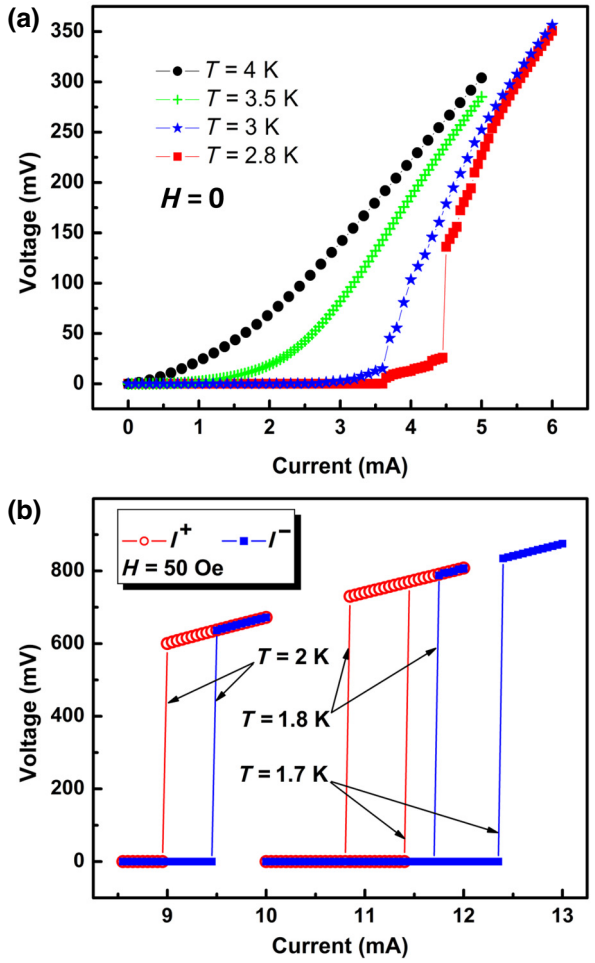

FIG. 3. (a) Voltage-current characteristics at different temperatures and $H = 0$. Measurements by a Quantum Design PPMS. (b) Voltage-current characteristics in a magnetic field H of 50 Oe for positive and negative directions of the direct current (I^+ and I^- are the corresponding critical-current amplitudes). Measurements by a Keithley 6221 current source and 2182A nanovoltmeter in the PPMS cryostat.

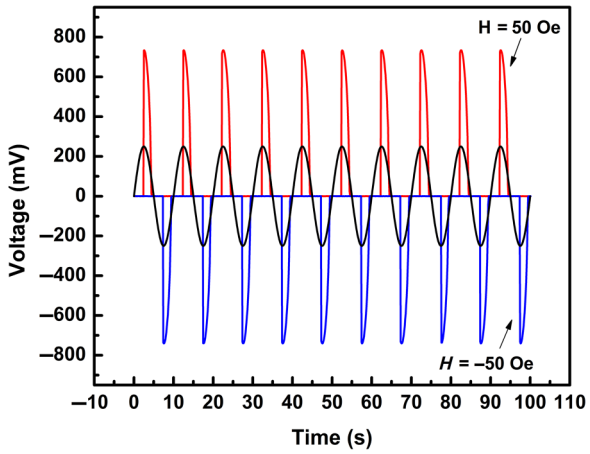

FIG. 4. Demonstration of superconducting-diode effect using a four-probe connection for both positive and negative external magnetic fields at $T = 2$ K. The alternating current (shown in arbitrary units) with $f = 0.1$ Hz is applied via contacts 1 and 3, and the voltage is measured between contacts 2 and 4 (see Fig. 2).

[Fig. 6(b)]. The situation changes when the control current is *on*. It generates a seed vortex or, possibly, even vortices, thus perturbing laminar supercurrent flow and generating initial turbulence, which facilitates massive flux inflow and a resistive state [Fig. 6(c)]. This, of course, is just a hypothesis of the mechanism, and rigorous modeling is required to explain both the generation and the extinction of the flux flow during this half-period of transport-current oscillation.

Let us try to confirm this hypothesis via the results presented in Figs. 2–5: these data allow us to draw explicit relations between the observations and to elucidate the facts, which are to some extent counterintuitive and interesting. As follows from Fig. 2(d), the normal-state resistance of the bridge is approximately 70 Ω. This is also consistent with Fig. 3(b), where the normal-state resistance can be recognized as the slope of the inclined line above the critical current at different temperatures. For example, for $T = 2$ K, the critical-current amplitude is between 9 and 9.5 mA and the voltage amplitude is in the range from 600 to 660 mV, values which are consistent with the aforementioned resistance value, and therefore the resistive state is fully spread over the entire bridge. This observation can be further extended to the diode state shown in Figs. 4 and 5, which also show similar values of current and voltage. The fact that the resistance during the diode action is built up within the total length of the bridge is in accordance with our aforementioned hypothesis and could have been expected. However, the more unexpected point is that the amplitude of the voltage triggered by the control current has the same magnitude as the amplitude of the voltage created by the overcritical alternating transport current. As follows from Fig. 2(c), the distance between auxiliary leads 5 and 6 (where the increase of the total current through the bridge occurs) is at least a factor of 6 smaller than the total length of the bridge. Therefore, we conclude that the local control current triggers a resistive state along the whole bridge, i.e., it has a *nonlocal* action.

This is an important corollary. To produce a similar triggering effect, if performed by a nonlocal increase of the main transport current through the bridge, would require more energy from the switching circuit. Obviously, the total impedance of the bridge is higher than the impedance of the small area traveled by the control current: the associated magnetic field amplitude is the same, but the volume is different. Thus, with a small applied energy, a large variation in circuit parameters is possible, for which the energy is being consumed from the transport current.

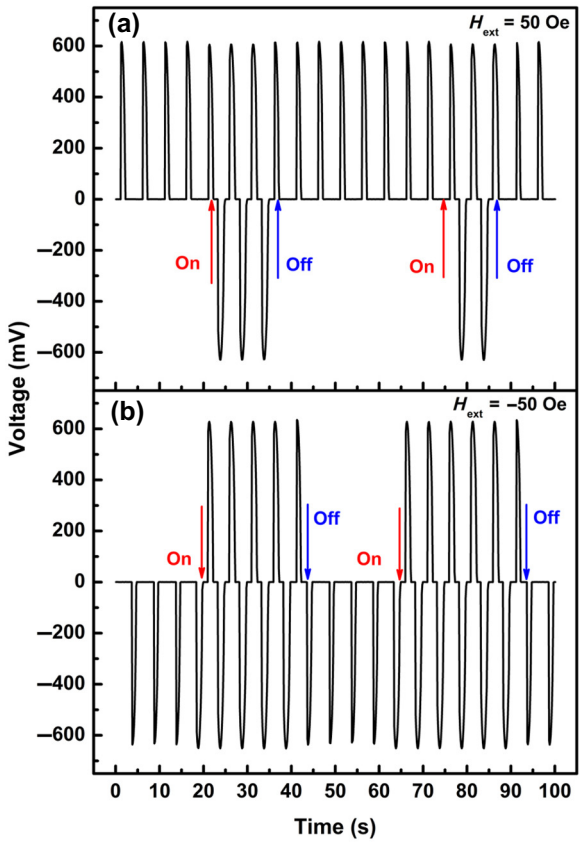

FIG. 5. Performance of the quadristor on application of the control current. The transport-current measurements were performed at $T = 2$ K via main leads 1–4, while the control current was supplied via auxiliary leads 5 and 6 [see Figs. 2(a)–2(c)]. The amplitude and frequency of the alternating transport current were 9.25 mA (a choice dictated by the results presented in Fig. 3) and 0.2 Hz, respectively. The control direct current was 2.5 mA (supplied by a Keithley 220 current source). The arrows indicate moments of time when the control current was switched *on* and *off*. Panels (a),(b) correspond to positive and negative external fields, $H = 50$ Oe and $H = -50$ Oe, respectively.

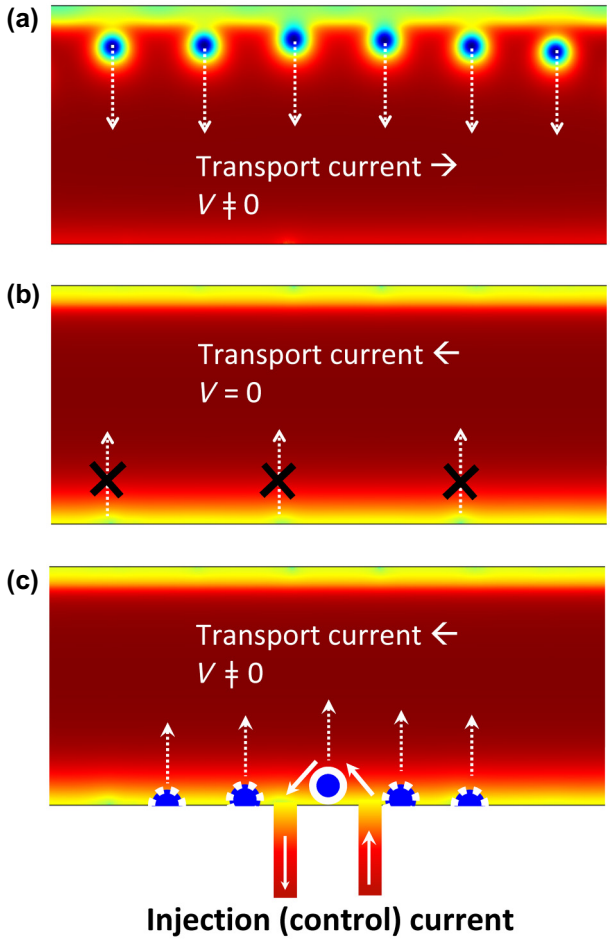

FIG. 6. Possible mechanism of quadristor operation. (a) Resistive state caused by the penetration of flux quanta through the Bean-Livingston barrier of the top ("weak") edge of the bridge. (b) This process is impossible at the bottom ("strong") edge during the subsequent half-period of alternating-current flow. (c) Current through auxiliary leads facilitates generation of the seed flux quantum and triggers the collective penetration through the whole bottom edge.

For the diode based on this mechanism, high-frequency operation has been demonstrated [23]. Thus, there are grounds to expect that the quadristor switching will also be functional at high frequencies. The investigation of this aspect, however, is beyond the scope of this article, which aimed to prove the overall operational principle of the device. Importantly, the amplitude of its control current ($I_{cntr} = 2.5$ mA) is much smaller than the amplitude of the alternating transport current: ($I_{tr} = 9.25$ mA). In future optimization of the quadristor parameters, the gain $g = I_{tr}/I_{cntr}$ may be further increased. However, even with the currently achieved value ($g \sim 3$–4), the quadristor can serve as a signal amplifier.

The quadristor performance resembles that of the planar transistor-type devices suggested recently in multiple articles [26–31]. However, in these devices, the design is based on different principles: for example, the field effect, which modifies the density of states, or the injection of high-energy electrons, which generates, for example, nonequilibrium phonon fluxes. These approaches require the application of potentials in the electronvolt range, which is above the intrinsic characteristic energy scale of superconductors (millielectronvolts). Noticeably, the auxiliary current (which could now be called the "control current") of our quadristor is much smaller than the transport current. Moreover, it is applied locally without increase of the total transport current. This provides grounds to expect that our device can be effectively used in circuits of superconducting microelectronics, such as logical elements and amplifiers.

V. CONCLUSION

To summarize, we demonstrated the possibility of reversible switching of the diode effect to the resistive regime in superconducting bridges. For that task, a Nb_3Sn bridge with superconducting-diode properties was fabricated with two auxiliary leads (whose separation is much shorter than the total bridge length) for injection of flux quanta. Injection of these quanta restores the symmetric oscillation regime to the alternating current. Very importantly, the ceasing of flux injection fully restores the superconducting regime during the half-period of oscillations, so the diode behavior is regained. If the relaxation mechanism of the restored diode state is similar to the SDE reported in [23], which is reasonable to suggest, one can thus expect high-frequency action not only for the diode but also for the quadristor. This effect may find practical applications after more explorations of its mechanism have been performed and functional regimes have been explored. Our finding also opens opportunities for studying the fundamental problems of nonequilibrium states in superconductors and interplay between turbulent motion and laminar motion in superfluid liquids. One obvious point that requires special studies is the discovered nonlocal action of the local control current.

ACKNOWLEDGMENTS

This work was supported by Office of Naval Research Grants No. N00014-21-1-2879 and No. N00014-20-1-2442. We are grateful to Physics Art Frontiers for the technical assistance provided, to R. Dulal for his help in the initial stage of this work, and to the anonymous referee of this article for valuable comments.

[1] Y. Tokura and N. Nagaosa, Nonreciprocal responses from non-centrosymmetric quantum materials, Nat. Commun. **9**, 3740 (2018).

[2] R. Wakatsuki and N. Nagaosa, Nonreciprocal Current in Noncentrosymmetric Rashba Superconductors, Phys. Rev. Lett. **121**, 026601 (2018).

[3] S. Hoshino, R. Wakatsuki, K. Hamamoto, and N. Nagaosa, Nonreciprocal charge transport in two-dimensional noncentrosymmetric superconductors, Phys. Rev. B **98**, 054510 (2018).

[4] F. Ando, Y. Miyasaka, T. Li, J. Ishizuka, T. Arakawa, Y. Shiota, T. Moriyama, Y. Yanase, and T. Ono, Observation of superconducting diode effect, Nature **584**, 373 (2020).

[5] T. Ideue and Y. Iwasa, One-way supercurrent achieved in an electrically polar film, Nature **584**, 349 (2020).

[6] C. Baumgartner, L. Fuchs, A. Costa, S. Reinhardt, S. Gronin, G. C. Gardner, T. Lindemann, M. J. Manfra, P. E. Faria Junior, D. Kochan, J. Fabian, N. Paradiso, and C. Strunk, Supercurrent rectification and magnetochiral effects in symmetric Josephson junctions, Nat. Nanotechnol. **17**, 39 (2022).

[7] H. Wu, Y. Wang, Y. Xu, P. K. Sivakumar, C. Pasco, U. Filippozzi, S. S. P. Parkin, Y.-J. Zeng, T. McQueen, and M. N. Ali, The field-free Josephson diode in a van der Waals heterostructure, Nature **604**, 653 (2022).

[8] E. Strambini, M. Spies, N. Ligato, S. Ilić, M. Rouco, C. González-Orellana, M. Ilyn, C. Rogero, F. S. Bergeret, J. S. Moodera, P. Virtanen, T. T. Heikkilä, and F. Giazotto, Superconducting spintronic tunnel diode, Nat. Commun. **13**, 2431 (2022).

[9] One more way of breaking the time-reversal symmetry was demonstrated recently by the Maeno group [32].

[10] N. F. Q. Yuan and L. Fu, Supercurrent diode effect and finite-momentum superconductors, Proc. Natl. Acad. Sci. **119**, e2119548119 (2022).

[11] S. Ilić and F. S. Bergeret, Theory of the Supercurrent Diode Effect in Rashba Superconductors with Arbitrary Disorder, Phys. Rev. Lett. **128**, 177001 (2022).

[12] A. Daido, Y. Ikeda, and Y. Yanase, Intrinsic Superconducting Diode Effect, Phys. Rev. Lett. **128**, 037001 (2022).

[13] T. Karabassov, I. V. Bobkova, A. A. Golubov, and A. S. Vasenko, Hybrid helical state and superconducting diode effect in superconductor/ferromagnet/topological insulator heterostructures, Phys. Rev. B **106**, 224509 (2022).

[14] J. J. He, Y. Tanaka, and N. Nagaosa, A phenomenological theory of superconductor diodes, New J. Phys. **24**, 053014 (2022).

[15] L. Bauriedl, C. Bäuml, L. Fuchs, C. Baumgartner, N. Paulik, J. M. Bauer, K.-Q. Lin, J. M. Lupton, T. Taniguchi, K. Watanabe, C. Strunk, and N. Paradiso, Supercurrent diode effect and magnetochiral anisotropy in few-layer $NbSe_2$, Nat. Commun. **13**, 4266 (2022).

[16] R. Wakatsuki, Y. Saito, S. Hoshino, Y. M. Itahashi, T. Ideue, M. Ezawa, Y. Iwasa, and N. Nagaosa, Nonreciprocal charge transport in noncentrosymmetric superconductors, Sci. Adv. **3**, e1602390 (2017).

[17] J. Shin, S. Son, J. Yun, G. Park, K. Zhang, Y. J. Shin, J.-G. Park, and D. Kim, Magnetic proximity-induced superconducting diode effect and infinite magnetoresistance in van der Waals heterostructure, arXiv:2111.05627 (2021).

[18] C. Baumgartner, L. Fuchs, A. Costa, J. Picó-Cortés, S. Reinhardt, S. Gronin, G. C. Gardner, T. Lindemann, M. J. Manfra, P. E. F. Junior, D. Kochan, J. Fabian, N. Paradiso, and C. Strunk, Effect of Rashba and Dresselhaus spin–orbit coupling on supercurrent rectification and magnetochiral anisotropy of ballistic Josephson junctions, J. Phys.: Condens. Matter **34**, 154005 (2022).

[19] Y. Hou, F. Nichele, H. Chi, A. Lodesani, Y. Wu, M. F. Ritter, D. Z. Haxell, M. Davydova, S. Ilić, F. S. Bergeret, A. Kamra, L. Fu, P. A. Lee, and J. S. Moodera, Ubiquitous superconducting diode effect in superconductor thin films, arXiv:2205.09276 (2022).

[20] D. Suri, A. Kamra, T. N. G. Meier, M. Kronseder, W. Belzig, C. H. Back, and C. Strunk, Non-reciprocity of vortex-limited critical current in conventional superconducting micro-bridges, Appl. Phys. Lett. **121**, 102601 (2022).

[21] M. K. Hope, M. Amundsen, D. Suri, J. S. Moodera, and A. Kamra, Interfacial control of vortex-limited critical current in type-II superconductor films, Phys. Rev. B **104**, 184512 (2021).

[22] D. Y. Vodolazov and F. M. Peeters, Superconducting rectifier based on the asymmetric surface barrier effect, Phys. Rev. B **72**, 172508 (2005).

[23] S. Chahid, S. Teknowijoyo, I. Mowgood, and A. Gulian, High-frequency diode effect in superconducting Nb_3Sn microbridges, Phys. Rev. B **107**, 054506 (2023).

[24] J. Mannhart, High-T_c transistors, Supercond. Sci. Technol. **9**, 49 (1996).

[25] D. Y. Vodolazov and F. M. Peeters, Rearrangement of the vortex lattice due to instabilities of vortex flow, Phys. Rev. B **76**, 014521 (2007).

[26] M. F. Ritter, A. Fuhrer, D. Z. Haxell, S. Hart, P. Gumann, H. Riel, and F. Nichele, A superconducting switch actuated by injection of high-energy electrons, Nat. Commun. **12**, 1266 (2021).

[27] M. F. Ritter, N. Crescini, D. Z. Haxell, M. Hinderling, H. Riel, C. Bruder, A. Fuhrer, and F. Nichele, Out-of-equilibrium phonons in gated superconducting switches, Nat. Electron. **5**, 71 (2022).

[28] G. De Simoni, F. Paolucci, P. Solinas, E. Strambini, and F. Giazotto, Metallic supercurrent field-effect transistor, Nat. Nanotechnol. **13**, 802 (2018).

[29] J. Chiles, E. G. Arnault, C.-C. Chen, T. F. Q. Larson, L. Zhao, K. Watanabe, T. Taniguchi, F. Amet, and G. Finkelstein, Non-reciprocal supercurrents in a field-free graphene Josephson triode, arXiv:2210.02644 (2022).

[30] M. Gupta, G. V. Graziano, M. Pendharkar, J. T. Dong, C. P. Dempsey, C. Palmstrøm, and V. S. Pribiag, Superconducting diode effect in a three-terminal Josephson device, arXiv:2206.08471 (2022).

[31] F. Paolucci, G. De Simoni, and F. Giazotto, A gate- and flux-controlled supercurrent diode effect, Appl. Phys. Lett. **122**, 042601 (2023).

[32] M. S. Anwar, T. Nakamura, R. Ishiguro, S. Arif, J. W. A. Robinson, S. Yonezawa, M. Sigrist, and Y. Maeno, Spontaneous superconducting diode effect in non-magnetic $Nb/Ru/Sr_2RuO_4$ topological junctions, arXiv:2211.14626 (2022).